Signal Processing 185 (2021) 108098

Contents lists available at ScienceDirect

Signal Processing

journal homepage: www.elsevier.com/locate/sigpro

Frequency estimation of a single real-valued sinusoid: An invariant function approach

Çağatay Candan*, Utku Çelebi

Department of Electrical and Electronics Engineering, Middle East Technical University (METU), Ankara 06800, Turkey

ARTICLE INFO

Article history:
Received 22 March 2020
Revised 18 February 2021
Accepted 25 March 2021
Available online 27 March 2021

Keywords:
Maximum likelihood estimation
Gridless search
Frequency estimation
Real-valued sinusoids
Parameter estimation

ABSTRACT

An invariant function approach for the computationally efficient (non-iterative and gridless) maximum likelihood (ML) estimation of unknown parameters is applied on the real-valued sinusoid frequency estimation problem. The main attraction point of the approach is its potential to yield a ML-like performance at a significantly reduced computational load with respect to conventional ML estimator that requires repeated evaluation of an objective function or numerical search routines. The numerical results indicate that the suggested estimator closely tracks the Cramer-Rao bound in the asymptotic region and performs very close to the ML estimator in other regions.

© 2021 Elsevier B.V. All rights reserved.

1. Introduction

The maximum likelihood frequency estimation of a sinusoid is a classical problem of statistical signal processing with important applications in array signal processing, spectrum estimation, communications, time-series analysis and others [1,2]. In this study, we present an alternative approach for the frequency estimation of real-valued sinusoids through invariant functions. The main advantage of the approach is its estimation accuracy in spite of its low computational complexity. Specifically for the frequency estimation problem, higher complexity methods utilize the maximum likelihood search, eigen or subspace decompositions, Kenefic and Nuttall [3], So et al. [4], So et al. [5]; while the suggested approach is based on transforming the input to Discrete Fourier Transform (DFT) domain and constructing a function of the Fourier spectrum samples which is *invariant* to the nuisance parameters of the problem.

The phrase of frequency estimation can refer to the parameter estimation problem for both complex-valued ($Ae^{j(\omega n+\phi)}$) and real-valued ($A\cos(\omega n+\phi)$) sinusoid signals with unknown amplitude, phase and frequency. For both real- and complex-valued sinusoids, the estimation of frequency is a non-linear parameter estimation problem; while the amplitude and phase estimation can be formulated as a linear estimation problem given the knowledge of frequency. The complex-valued sinusoids are in general the low-pass equivalent of a band-pass signal and utilized in spectrum modelling, direction of arrival estimation, communications problems. There are several methods for the parameter estimation of complex-valued sinusoids (also called complex exponentials) [2]. Among them, Quinn [6], Quinn and Hannan [7], Macleod [8], Aboutanios and Mulgrew [9], Jacobsen and Kootsookos [10], Candan [11,12], Liao and Lo [13], Orguner and Candan [14], Belega and Petri [15], Fan and Qi [16], Chen et al. [17] overlap with the invariant function approach described herein where the goal is to develop a very low complexity estimator for this fundamental problem. For example, the unknown frequency $\omega = 2\pi(k_p+\delta)/N$ is estimated in two-stages in Quinn [6], Quinn and Hannan [7], Macleod [8], Aboutanios and Mulgrew [9], Jacobsen and Kootsookos [10], Candan [11], 12], Liao and Lo [13], Orguner and Candan [14], Belega and Petri [15], Fan and Qi [16], Chen et al. [17]. In the first stage N-point DFT of the input is calculated and the DFT index with the peak magnitude is declared as $\widehat{k}_p$ (also see Fig. 1). In the second stage (the fine frequency estimation stage), the remaining unknown δ (fine frequency part) is estimated through the relation

$$\widehat{\delta} = f^{-1}\left(\mathrm{Re}\left\{\frac{R[\widehat{k}_p-1]-R[\widehat{k}_p+1]}{2R[\widehat{k}_p]-R[\widehat{k}_p-1]-R[\widehat{k}_p+1]}\right\}\right) \tag{1}$$

where $f^{-1}(\cdot)$ refers to the inverse function of $f(\delta) = \tan(\pi\delta/N)/\tan(\pi/N)$ and $R[\cdot]$ is the N-point DFT samples, as illustrated in Fig. 1.[1] The complexity of the estimator given by

* Corresponding author.
E-mail addresses: ccandan@metu.edu.tr (Ç. Candan), ucelebi@metu.edu.tr (U. Çelebi).

[1] The estimator in (1) is selected as an illustrative example of its class due to the algebraic simplicity of $f(\cdot)$ function in its expression [11,12].

https://doi.org/10.1016/j.sigpro.2021.108098
0165-1684/© 2021 Elsevier B.V. All rights reserved.

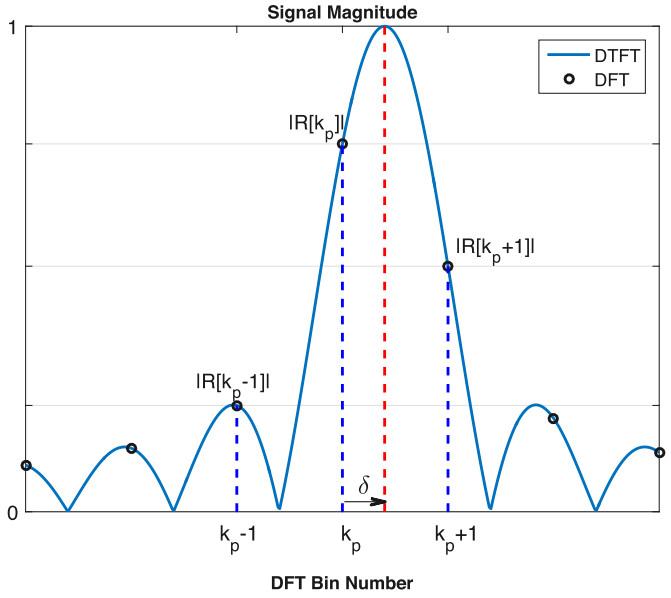

Fig. 1. An illustration for the first stage of the proposed method

(1) comprises of i. calculation of N-point DFT, ii. calculation of ratio appearing in the argument of $f^{-1}(\cdot)$, iii. evaluation of the inverse function. In spite of its extreme low complexity, the performance of the estimator is surprisingly good [12].

The history of two-stage estimators dates back to early 1950's to the works of Woodward and Kotelnikov, with their application in radar range measurement [18] and pulse position/frequency modulation systems [19], according to the note in the classical textbook of Van Trees, [20, p.278]. In the context of frequency estimation, Bartlett is among the first to suggest the usage of DFT samples for the frequency estimation in Bartlett [21, Appendix 1]; but Bartlett does not develop the details of his suggestion. Rife et al. explicitly describe the coarse- and fine- search stages for the frequency estimation problem in 1970's and propose a fine-frequency estimator based on the magnitude of the DFT samples in Rife and Vincent [22, Method 2] and suggest to use a numerical search based solution via the secant method in Rife and Boorstyn [23, Section IV]. In early 1990's, Quinn have developed several computationally efficient and highly accurate fine frequency estimators [6,24]. A complete account of these estimators and their performance analyses in terms of asymptotic MSE, threshold behaviour and much more is given by Quinn and Hannan [7]. In early 2000's, Aboutanios have developed several novel fine-frequency estimators for N-point and 2N-point DFT samples in his Ph.D. work [25]. Among the suggested methods of Aboutanios, the estimator today known as Aboutanios and Mulgrew estimator stands out with its high accuracy and low computational complexity [9]. In recent years, the literature on the fine-frequency estimators has been extended to the real/complex valued sinusoids with/without windowing operation via processing of 2, 3 or more DFT samples [10–17]. All of these methods mainly differ in the non-linear expression used in the fine-frequency estimation stage. In this study, we refer the functions $f(\cdot)$ involved in the fine-frequency estimation stage, such as the one in (1), as the invariant function.

The frequency estimation for real-valued sinusoids is a bit more complicated than its complex-valued counterpart due to the interaction of two complex-valued sinusoids forming the real-valued sinusoid. In literature, conventional linear prediction based approaches have been extended to the case of real-valued sinusoids in So et al. [4], Chan et al. [26], So et al. [27]. Sub-space based methods have been developed in So et al. [5] and recently, some low-complexity estimators have been proposed [28,29]. Different from earlier efforts, the low complexity estimators suggested in the literature aim to cancel one of complex exponentials forming the cosine waveform and following the cancellation operation, well known invariant function based estimators for the complex exponentials are utilized. For example, the method of Djukanovicàims to eliminate one of the complex exponentials forming $\cos(\omega n+\phi)=(e^{j\omega n+\phi}+e^{-j\omega n-\phi})/2$ by filtering [28]. To do the elimination, a rough frequency estimate is generated and the complex exponential with the negative valued frequency is filtered. The method of Ye et al. [29,30] is based on a similar principle and estimates not only frequency, but also the amplitude and phase to implement an interference cancellation procedure.

Different from existing low complexity estimators, we suggest an approach based on an invariant function for the real-valued sinusoid frequency estimation problem in complete analogy with the ones for the complex exponentials. The suggested estimator requires the inverse mapping $f^{-1}(\cdot)$ for the developed invariant function. The inverse mapping is independent of data and can be calculated offline and stored as a look-up table or the inverse function can be computed online via a Taylor series based scheme at a very low complexity. It should be underlined that the suggested scheme uses iterations only for the online evaluation of the inverse function via Taylor series, similar to the numerical evaluation of any transcendental function. Hence, we suggest a gridless, non-iterative (in terms of data processing), very low computational complexity estimator with a ML-like performance for the real-valued sinusoid frequency estimation problem.

2. Preliminaries

A sampled sinusoidal signal with an unknown amplitude A, phase ϕ and frequency ω is observed under zero mean additive white Gaussian noise (AWGN) $w[n]$ with variance σ_w^2,

$$r[n]=A\cos(\omega n+\phi)+w[n],\quad n=\{0,\dots,N-1\}. \tag{2}$$

We consider the amplitude and the phase of the sinusoid as the nuisance parameters and treat the frequency ω as the sole parameter of interest. In fact, since $r[n]$ can be written as $r[n]=A_c\cos(\omega n)+A_s\sin(\omega n)+w[n]$ with $A_c=A\cos(\phi)$, $A_s=-A\sin(\phi)$; the maximum likelihood estimation of amplitude and phase reduces to a simpler problem with a linear observation model given the frequency estimate. The signal-to-noise-ratio (SNR) definition adopted in this study is $\mathrm{SNR}=A^2/(2\sigma_w^2)$.

2.1. Maximum-likelihood (ML) estimator

After some elementary manipulations outlined in Appendix A, the maximum-likelihood estimate of frequency is expressed as

$$\hat{\omega}_{\mathrm{ML}}=\arg\max_{\omega}\frac{|R(e^{j\omega})|^2-\frac{\sin(\omega N)}{N\sin(\omega)}\mathrm{Re}\left\{R^2(e^{j\omega})e^{j\omega(N-1)}\right\}}{N-\frac{\sin^2(\omega N)}{N\sin^2(\omega)}}. \tag{3}$$

Here $R(e^{j\omega})=\sum_{n=0}^{N-1}r[n]e^{-j\omega n}$ is the discrete-time Fourier transform (DTFT) of the input. The ML expression for the same problem also appears in Kay [31, Eq. (7.65)] and [3]. Different from these expressions, (3) presents the relation in terms of DTFT of the input resulting in a simpler expression.

A straightforward implementation of the ML estimator in (3) is the application fast Fourier transform (FFT) for the calculation of DTFT samples and execution of a search for the likelihood maxima. Interestingly, the peak location of the energy spectra, $\arg\max_{\omega}|R(e^{j\omega})|^2$, is not the maximum likelihood estimate for a finite N. Yet, as the number of observations N increases, the ML estimator converges to the peak localization in the magnitude DTFT spectra (periodogram). To reduce the computational complexity, a

chirp-z transform based DTFT calculation over a portion of the spectrum can be also implemented. In this study, our goal is to present a much lower complexity estimator which is almost as good as the ML estimator given by (3).

2.2. Cramer-Rao bound

For finite N, the Cramer-Rao bound (CRB) for the real-valued sinusoid depends on the nuisance parameter set (amplitude and phase) and on the parameter of interest (frequency). As $N \to \infty$, the term $\sum_{n=0}^{N-1} \sin(2\omega n + 2\phi)$ appearing in the Fisher information matrix (FIM) entries given in Kay [31, p. 56] approaches 0 and CRB becomes independent of phase and frequency. The bound as $N \to \infty$ is called the asymptotic Cramer-Rao bound (ACRB):

$$E\{(\omega - \hat{\omega})^2\} \geq \text{ACRB} = \frac{12}{\text{SNR}(N^2-1)N}, \text{ as } N \to \infty. \tag{4}$$

We also note that the ACRB expression in (4) coincides with the hybrid Cramer-Rao bound (HCRB) expression for finite N provided that the signal phase is taken as a uniformly distributed random variable in $[0, 2\pi)$. HCRB is a Bayesian performance bound utilized in the presence of random nuisance parameters, [32]. In the numerical results section, we randomize the phase ϕ and utilize HCRB (i.e. the ACRB expression in (4)) as a performance benchmark. Since the value of phase can significantly affect the performance, its non-informative randomization results in a fair performance comparison for the frequency estimation problem. Lastly, we prefer to express the ACRB expression with the units of DFT bins. This unit convention is further explained in Section 4.

3. Proposed method

The proposed method is composed of two stages. The first stage is the calculation of $2N$-point DFT of the input $r[n] = A\cos\left(\frac{2\pi}{2N}(k_p+\delta)n + \phi\right) + w[n]$, $n = \{0, \ldots, N-1\}$. Note that we have switched the notation for the frequency variable from ω to $\frac{2\pi}{2N}(k_p+\delta)$. Here $k_p + \delta$ denotes the frequency in terms of $2N$-point DFT bins where k_p is an integer between 0 and N and δ is a real number in $(-0.5, 0.5]$ (also see Fig. 1). The first stage output is the DFT bin index with the maximum magnitude. This index is denoted by $\widehat{k}_p$, as shown in Algorithm 1 listing. In essence, the first stage implements a coarse search for the frequency via periodogram. Since the search is coarse, there is no need to utilize the exact ML expression (3) in this stage. (Interested readers can also examine earlier works on the frequency estimation of complex exponential signals utilizing the same model for more information, Quinn [6], Quinn and Hannan [7], Macleod [8], Aboutanios and Mulgrew [9], Jacobsen and Kootsookos [10], Candan [11], 12], Liao and Lo [13], Orguner and Candan [14], Belega and Petri [15], Fan and Qi [16].)

The second stage, fine frequency estimation stage, utilizes three DFT outputs with the indices $\{\widehat{k}_p - 1, \widehat{k}_p, \widehat{k}_p + 1\}$ to estimate δ, as shown in Fig. 1. To produce the fine frequency estimate $\widehat{\delta}$, a non-linear function of three arguments is constructed and this function is evaluated with the arguments of $R[\widehat{k}_p + l]$, $l = \{-1, 0, 1\}$. The operation is, in principle, similar to the one given by (1). The final estimate for the frequency becomes $\widehat{k}_p + \widehat{\delta}$ with the unit of DFT bins or $\widehat{\omega} = \frac{2\pi}{2N}(\widehat{k}_p + \widehat{\delta})$ radians per sample.

The performance of the proposed method critically depends on the non-linear function at the fine frequency estimation stage. By design, this function should be invariant to the nuisance parameters of problem in the absence of noise. To illustrate the invariant function, let's examine the complex exponential signal model with $r[n] = A\exp(j(\omega n + \phi)) + w[n]$, $n = \{0, \ldots, N-1\}$. In the absence of noise, DFT of $r[n]$ becomes $R[k] = A\exp(j\phi)\text{DFT}\{\exp(j\omega n)\}$. It can be noticed that the insertion of $R[k]$ in (1) results in the cancellation of $A\exp(j\phi)$ terms appearing on the numerator and denominator of ratio in the argument of the real part operator. Hence, this ratio is invariant to amplitude A and phase ϕ. Trivially, a function of this ratio is also an invariant function. It is possible to suggest different invariant functions for the same problem [6,8–16]. The estimator performance critically depends on the properties of the invariant function, i.e. some invariant functions are more successful in the tracking of the Cramer-Rao bound such as the one proposed by Aboutanios and Mulgrew [9].

Algorithm 1: Proposed method, (see [35] for a ready-to-use MATLAB implementation).

Input : $r[n]$: N samples of noisy real-valued sinusoid;
Output: $\widehat{\omega} = \frac{2\pi}{2N}(\widehat{k}_p + \widehat{\delta}_\text{F})$ rad./sample;
$R[k]$ =fft$(r[n], 2N)$ ($2N$-point FFT calculation);
$\widehat{k}_p = \underset{0\leq k\leq N-1}{\arg\max}\ |R[k]|^2$(locate maxima in spectrum);
Set $\widetilde{R}[l] = R[l + \widehat{k}_p]e^{j\frac{\pi(N-1)}{2N}(l+\widehat{k}_p)}$, $l = \{-1, 0, 1\}$;
Set $\widetilde{R}_\text{re}[l] = \text{Re}\{\widetilde{R}[l]\}$ and$\widetilde{R}_\text{im}[l] = \text{Im}\{\widetilde{R}[l]\}$;
Evaluate ratio$_\text{re}$ and ratio$_\text{im}$; use (9)
if lookup-table exists,
    $\widehat{\delta}_\text{re} = f_\text{re}^{-1}(\text{ratio}_\text{re})$, $\widehat{\delta}_\text{im} = f_\text{im}^{-1}(\text{ratio}_\text{im})$
else
    Set $\delta_\text{re}^0 = 0.25$, $\delta_\text{im}^0 = 0.25$ and maxiter $= 10$;
    for iteration from 1 to maxiter,
        $\widehat{\delta}_\text{re} = f_\text{re}^{-1}(\text{ratio}_\text{re}, \delta_\text{re}^0)$; use (14)
        $\widehat{\delta}_\text{im} = f_\text{im}^{-1}(\text{ratio}_\text{im}, \delta_\text{im}^0)$;
        Set $\delta_\text{re}^0 = \widehat{\delta}_\text{re}$ and $\delta_\text{im}^0 = \widehat{\delta}_\text{im}$;
    end for
end
Evaluate the fusion coefficient α; use (16)
$\widehat{\delta}_\text{F} = \alpha\widehat{\delta}_\text{re} + (1-\alpha)\widehat{\delta}_\text{im}$;
Return $\widehat{\omega} = \frac{2\pi}{2N}(\widehat{k}_p + \widehat{\delta}_\text{F})$.

3.1. Constructing invariant function for real-valued sinusoids

In the absence of noise, $2N$-point DFT of the input,

$$R[k] = \sum_{n=0}^{N-1} r[n]e^{-j\frac{2\pi}{2N}nk} = A\sum_{n=0}^{N-1}\cos\left(\frac{2\pi}{2N}(k_p+\delta)n + \phi\right)e^{-j\frac{2\pi}{2N}nk} \tag{5}$$

can be expressed as

$$R[k] = \frac{A}{2}e^{-j\frac{\pi(N-1)}{2N}k}\left(\cos(\widetilde{\phi})\left[\frac{\sin\left(\frac{\pi(k_p-k+\delta)}{2}\right)}{\sin\left(\frac{\pi(k_p-k+\delta)}{2N}\right)} + \frac{\sin\left(\frac{\pi(k_p+k+\delta)}{2}\right)}{\sin\left(\frac{\pi(k_p+k+\delta)}{2N}\right)}\right]\right.$$
$$\left. + j\sin(\widetilde{\phi})\left[\frac{\sin\left(\frac{\pi(k_p-k+\delta)}{2}\right)}{\sin\left(\frac{\pi(k_p-k+\delta)}{2N}\right)} - \frac{\sin\left(\frac{\pi(k_p+k+\delta)}{2}\right)}{\sin\left(\frac{\pi(k_p+k+\delta)}{2N}\right)}\right]\right) \tag{6}$$

where $\widetilde{\phi} = \phi + \frac{\pi}{2N}(k_p+\delta)(N-1)$, after some elementary manipulations.

In the absence of noise or at high SNR, the first stage output $\widehat{k}_p$ exactly matches the integer part of the unknown frequency, that is $\widehat{k}_p = k_p$. More specifically, it is known from the literature that above a certain SNR value, called the threshold SNR, the coarse search result exactly matches the true frequency bin k_p with an overwhelming probability [7,33,34]. The SNR region above the threshold SNR value is referred as the high SNR region or the asymptotic region in the literature. Hence, with the high SNR region assumption, which implies $\widehat{k}_p = k_p$, the DFT outputs with the

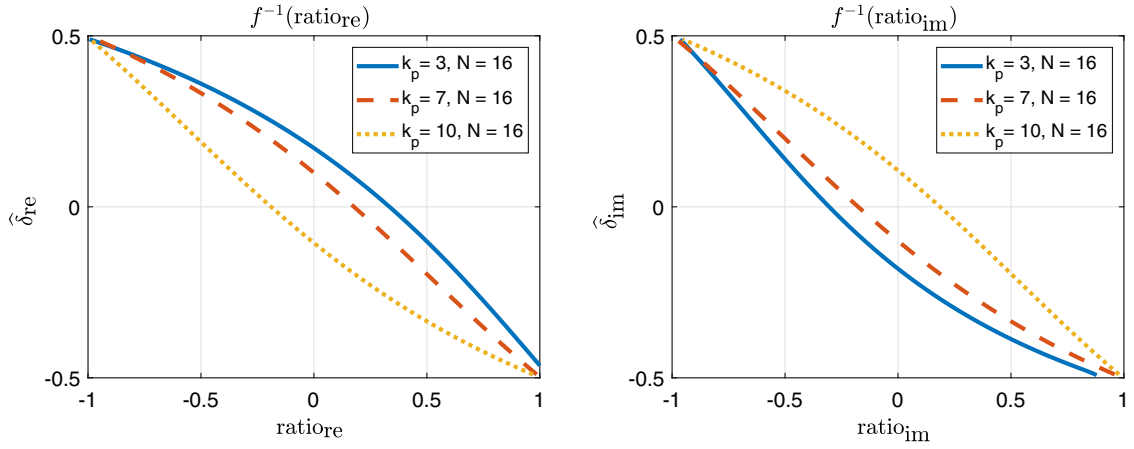

(a) $f_{\text{re}}^{-1}(\text{ratio}_{\text{re}})$ (b) $f_{\text{im}}^{-1}(\text{ratio}_{\text{im}})$

Fig. 2. Inverse of the invariant functions $f_{\text{re}}(\cdot)$ and $f_{\text{im}}(\cdot)$ for a look-up table implementation.

indices $\{k_p-1, k_p, k_p+1\}$, are assumed to be used in the development of the fine-frequency estimator. Here $l \triangleq k-k_p$, denotes the offset from the index k_p or more generally the offset from the index $\widehat{k}_p$ which is the first stage output.

Next, we define the phase corrected version of the $2N$-point DFT outputs as

$$\widetilde{R}[l] = R[k]e^{j\frac{\pi(N-1)}{2N}k}|_{k=l+k_p} = R[l+k_p]e^{j\frac{\pi(N-1)}{2N}(l+k_p)} \tag{7}$$

and denote the real and imaginary parts of $\widetilde{R}[l] = \widetilde{R}_{\text{re}}[l] + j\widetilde{R}_{\text{im}}[l]$ as $\widetilde{R}_{\text{re}}[l]$ and $\widetilde{R}_{\text{im}}[l]$, respectively. From (6), $\widetilde{R}_{\text{re}}[l]$ and $\widetilde{R}_{\text{im}}[l]$ can be expressed as

$$\widetilde{R}_{\text{re}}[l] \triangleq \text{Re}\{\widetilde{R}[l]\} = M_{\text{re}}\left[\frac{\sin\left(\frac{\pi(\delta-l)}{2}\right)}{\sin\left(\frac{\pi(\delta-l)}{2N}\right)} + \frac{\sin\left(\frac{\pi(2k_p+l+\delta)}{2}\right)}{\sin\left(\frac{\pi(2k_p+l+\delta)}{2N}\right)}\right],$$

$$\widetilde{R}_{\text{im}}[l] \triangleq \text{Im}\{\widetilde{R}[l]\} = M_{\text{im}}\left[\frac{\sin\left(\frac{\pi(\delta-l)}{2}\right)}{\sin\left(\frac{\pi(\delta-l)}{2N}\right)} - \frac{\sin\left(\frac{\pi(2k_p+l+\delta)}{2}\right)}{\sin\left(\frac{\pi(2k_p+l+\delta)}{2N}\right)}\right], \tag{8}$$

where $M_{\text{re}} = \frac{A}{2}\cos(\widetilde{\phi})$ and $M_{\text{im}} = \frac{A}{2}\sin(\widetilde{\phi})$. Here $\widetilde{\phi} = \phi + \frac{\pi}{2N}(k_p+\delta)(N-1)$ is a constant depending on the unknown parameters, but independent of l.

Temporarily focusing on $\widetilde{R}_{\text{re}}[l]$, it can be easily verified that the following expression involving $\widetilde{R}_{\text{re}}[l]$, $l=\{-1,0,1\}$ is invariant to the nuisance parameters of the problem, namely the signal amplitude and phase,

$$\text{ratio}_{\text{re}} \triangleq \frac{\widetilde{R}_{\text{re}}[1]-\widetilde{R}_{\text{re}}[-1]}{2\widetilde{R}_{\text{re}}[0]-\widetilde{R}_{\text{re}}[1]-\widetilde{R}_{\text{re}}[-1]} \triangleq f_{\text{re}}(\delta). \tag{9}$$

Stated differently, the ratio_{re} given by (9) is solely a function of δ in the absence of noise. We emphasize this fact with the notation of $\text{ratio}_{\text{re}} = f_{\text{re}}(\delta)$ in (9).

We also use the same invariant relation form for the imaginary part of DFT outputs given in (8) and define

$$\text{ratio}_{\text{im}} \triangleq \frac{\widetilde{R}_{\text{im}}[1]-\widetilde{R}_{\text{im}}[-1]}{2\widetilde{R}_{\text{im}}[0]-\widetilde{R}_{\text{im}}[1]-\widetilde{R}_{\text{im}}[-1]} \triangleq f_{\text{im}}(\delta). \tag{10}$$

Note that $f_{\text{re}}(\delta) \neq f_{\text{im}}(\delta)$ due to the sign difference in the second component of the sum (8) in the definition of $\widetilde{R}_{\text{re}}[l]$ and $\widetilde{R}_{\text{im}}[l]$.

Assuming that the inverse mapping for the invariant functions, $f_{\text{re}}^{-1}(\cdot)$ or $f_{\text{im}}^{-1}(\cdot)$, exists; an estimate for δ can be generated, in principle, via the application of the inverse function on the ratios, say $\widehat{\delta}_{\text{re}} = f_{\text{re}}^{-1}(\text{ratio}_{\text{re}})$. Fig. 2 shows the inverse mappings $f_{\text{re}}^{-1}(\text{ratio}_{\text{re}})$ and $f_{\text{im}}^{-1}(\text{ratio}_{\text{im}})$ for different parameter settings of N and k_p. Unfortunately, there is no simple analytical expression for the inverse function for the suggested invariant function. Hence, we need to utilize either a look-up table or numerical techniques for the inverse function mapping. Below, we describe a numerical procedure for the inverse function mapping when the look-up table approach is not feasible or simply not preferred, say to achieve a better numerical accuracy.

3.2. Inversion of invariant function

In [12], a similar invariant function for the frequency estimation of *complex exponentials* is given as $f(\delta) = \tan(\pi\delta/N)/\tan(\pi/N)$ as given in (1). For the complex exponential problem, it is possible to express the inverse function analytically in terms of elementary functions; but this is not the case for the one suggested in (9). Fig. 2 shows the inverse of the invariant functions for different k_p and N values. Different from the complex exponential problem, the invariant function for the real-valued sinusoid depends on both k_p and N. Below, we describe a general, Taylor series based iterative method to establish the inverse mapping.

Focusing on the ratio_{re} given in (9), we consider $\widetilde{R}_{\text{re}}[l]$, $l=\{-1,0,1\}$ as a function of δ and expand the function around an arbitrary non-zero $\delta=\delta_0$ via the Taylor series and retain only the first two terms of the series. The approximation can be expressed as $\widetilde{R}_{\text{re}}[l] \approx K_l + \dot{K}_l(\delta-\delta_0)$. Here $K_l = \widetilde{R}_{\text{re}}[l]|_{\delta=\delta_0}$ and $\dot{K}_l = \frac{d}{d\delta}\widetilde{R}_{\text{re}}[l]\big|_{\delta=\delta_0}$ can be explicitly given as

$$K_l = M_{\text{re}}\left[h\left(\frac{\pi(\delta_0-l)}{2}\right) + h\left(\frac{\pi(2k_p+l+\delta_0)}{2}\right)\right] \tag{11}$$

$$\dot{K}_l = \frac{\pi}{2}M_{\text{re}}\left[h'\left(\frac{\pi(\delta_0-l)}{2}\right) + h'\left(\frac{\pi(2k_p+l+\delta_0)}{2}\right)\right]$$

where $h(x) = \sin(x)/\sin(x/N)$ and $h'(x) = \frac{d}{dx}h(x) = \frac{N\cos(x)\sin(x/N)-\sin(x)\cos(x/N)}{N\sin^2(x/N)}$.

By substituting the Taylor series approximations for $\{\widetilde{R}_{\text{re}}[-1], \widetilde{R}_{\text{re}}[0], \widetilde{R}_{\text{re}}[1]\}$ in (9), we get

$$\text{ratio}_{\text{re}} \approx \frac{A_{\text{re}} + \dot{A}_{\text{re}}(\delta-\delta_0)}{B_{\text{re}} + \dot{B}_{\text{re}}(\delta-\delta_0)}, \tag{12}$$

where $A_{\text{re}} = K_1 - K_{-1}$, $\dot{A}_{\text{re}} = \dot{K}_1 - \dot{K}_{-1}$ and $B_{\text{re}} = 2K_0 - K_1 - K_{-1}$, $\dot{B}_{\text{re}} = 2\dot{K}_0 - \dot{K}_1 - \dot{K}_{-1}$.

To facilitate a simple approximation for $f_{\text{re}}^{-1}(\delta)$, valid around $\delta = \delta_0$; we multiply the numerator and denominator of the ratio on the right side of (12) by $B_{\text{re}} - \dot{B}_{\text{re}}(\delta - \delta_0)$ and ignore all second order terms to get,

$$\text{ratio}_{\text{re}} \approx \frac{A_{\text{re}}}{B_{\text{re}}} + \frac{\dot{A}_{\text{re}}B_{\text{re}} - A_{\text{re}}\dot{B}_{\text{re}}}{B_{\text{re}}^2}(\delta - \delta_0). \tag{13}$$

From (13), the unknown δ can be solved as

$$\widehat{\delta}_{\text{re}} = \frac{B_{\text{re}}^2}{\dot{A}_{\text{re}}B_{\text{re}} - A_{\text{re}}\dot{B}_{\text{re}}}\left(\text{ratio}_{\text{re}} - \frac{A_{\text{re}}}{B_{\text{re}}}\right) + \delta_0. \tag{14}$$

In practice, the inversion operation is applied iteratively; that is, we use the result of an earlier iteration as the expansion point (δ_0) of the next iteration. With the iterative operation, the inverse mapping becomes a non-linear function of ratio_{re}. The accuracy of the suggested iterative inversion scheme is examined in the numerical results section. A detailed implementation is available in Candan and Celebi [35].

The same arguments can be repeated verbatim for the inversion of $f_{\text{im}}(\delta)$ function. Hence, a second estimate can be generated from the imaginary parts of $\widetilde{R}[l]$, $l = \{-1, 0, 1\}$ via the relation $\widehat{\delta}_{\text{im}} = \frac{B_{\text{im}}^2}{\dot{A}_{\text{im}}B_{\text{im}} - A_{\text{im}}\dot{B}_{\text{im}}}\left(\text{ratio}_{\text{im}} - \frac{A_{\text{im}}}{B_{\text{im}}}\right) + \delta_0$. where $A_{\text{im}}, \dot{A}_{\text{im}}$ and $B_{\text{im}}, \dot{B}_{\text{im}}$ are defined similarly.

3.3. Independence of $\widehat{\delta}_{re}$ and $\widehat{\delta}_{im}$

As shown by Quinn [36], the real and imaginary parts of $2N$-point DFT output calculated at step 1 of Algorithm 1 listing are correlated. Yet, as shown in (Appendix B), once the phase correction step of Algorithm 1 (step 3) is executed, the resultant real and imaginary parts (step 4) become independent. Hence, the estimates, $\widehat{\delta}_{\text{re}}$ and $\widehat{\delta}_{\text{im}}$, which are derived solely from real and imaginary parts of $\widetilde{R}[l]$ (steps 5 to 15) are also independent random variables. This important result enables us to utilize a simple fusion rule for uncorrelated random variables as shown in the step 17 of Algorithm 1 Listing. We believe that the phase correction operation at step 3, decorrelating real and imaginary parts, can be useful in other applications involving zero-padded DFTs. In addition, different versions of estimate fusion have been previously studied by Quinn and Hannan, such as [7, Algorithm 5, p.197] or [7, Algorithm 4, p.188], in their influential research monograph. The fusion strategy in this study can be interpreted as an effort along the same line of thought.

3.4. Fusing estimates

The final step of the suggested method is the fusion of the estimates produced from the real and imaginary parts of $\widetilde{R}[l]$. The estimates $\widehat{\delta}_{\text{re}}$ and $\widehat{\delta}_{\text{im}}$ are combined to reduce the estimation error. By construction, $\widetilde{R}_{\text{re}}[l]$ and $\widetilde{R}_{\text{im}}[l]$ are independent Gaussian random variables with variance $\sigma_w^2 N/2$, as shown in (Appendix B). Other results of importance from (Appendix B) are as follows: The cross-correlation of $\widetilde{R}_{\text{re}}[l_1]$ and $\widetilde{R}_{\text{im}}[l_2]$ is zero for all (l_1, l_2) pairs. Yet $\widetilde{R}_{\text{re}}[l_1]$ is correlated with $\widetilde{R}_{\text{re}}[l_2]$ for odd valued $l_1 - l_2$. The same is also true for $\widetilde{R}_{\text{im}}[l_1]$. The most important fact for fusion purposes is that the estimates $\widehat{\delta}_{\text{re}}$ and $\widehat{\delta}_{\text{im}}$, derived from $\widetilde{R}_{\text{re}}[l]$ and $\widetilde{R}_{\text{im}}[l]$ respectively, are independent random variables. To combine them, we suggest to apply the best linear unbiased estimator (BLUE) rule which is applicable for uncorrelated random variables.

From (8), it can be noted that the input SNR for the estimates $\widehat{\delta}_{\text{re}}$ and $\widehat{\delta}_{\text{im}}$ are determined by the factors $M_{\text{re}} = \frac{A}{2}\cos(\widetilde{\phi})$ and $M_{\text{im}} = \frac{A}{2}\sin(\widetilde{\phi})$, respectively. Depending on the unknown parameter $\widetilde{\phi}$; SNR and therefore the accuracy of the estimates $\widehat{\delta}_{\text{re}}$ and $\widehat{\delta}_{\text{im}}$ can vary significantly. We suggest to use the following linear unbiased fusion rule to generate the final estimate $\widehat{\delta}_{\text{F}}$,

$$\widehat{\delta}_{\text{F}} = \alpha\widehat{\delta}_{\text{re}} + (1 - \alpha)\widehat{\delta}_{\text{im}}. \tag{15}$$

The fusion coefficient α should be ideally selected as $\alpha_{\text{ideal}} = M_{\text{re}}^2/(M_{\text{re}}^2 + M_{\text{im}}^2) = \cos^2(\widetilde{\phi})$. Yet, the signal phase is a nuisance parameter which is not estimated in the invariant function setting. Instead, we suggest to use the following approximation to the ideal fusion coefficient

$$\alpha \triangleq \frac{\widetilde{R}_{\text{re}}^2[0]}{\widetilde{R}_{\text{re}}^2[0] + \widetilde{R}_{\text{im}}^2[0]} = \left(1 + \left(\frac{\widetilde{R}_{\text{im}}[0]}{\widetilde{R}_{\text{re}}[0]}\right)^2\right)^{-1}. \tag{16}$$

The approximation can be justified by noting from (8) that

$$\frac{\widetilde{R}_{\text{im}}[0]}{\widetilde{R}_{\text{re}}[0]} = \tan(\widetilde{\phi})\underbrace{\left[\tan\left(\frac{\pi k_p}{2N}\right)\cot\left(\frac{\pi(k_p + \delta)}{2N}\right)\right]^p}_{\approx 1} \approx \tan(\widetilde{\phi}),$$

for $N \gg 1$ and $k_p \gg 1$. Here $p = (-1)^{\widehat{k}_p}$ is the parity of $\widehat{k}_p$ (first stage output), taking the value of 1 or -1 depending on $\widehat{k}_p$ is an odd or even integer, see (Appendix C) for details.

Finally, the suggested fusion coefficient, given by (16), can be expressed as $\alpha \approx \left(1 + \tan^2(\widetilde{\phi})\right)^{-1} = \cos^2(\widetilde{\phi})$ for $N \gg 1$ and $k_p \gg 1$. This concludes the derivation of the estimator given in Algorithm 1.

3.5. Estimator MSE at High SNR

The MSE at high SNR can be written as $E\{(\delta - \widehat{\delta}_F)^2\} = \frac{f_{\text{re}} + f_{\text{im}}}{\text{SNR}}$, where $f_{\text{re}} = \frac{NB_{\text{re}}^2 - 2A_{\text{re}}B_{\text{re}}\rho + \sigma_{\text{re}}^2 A_{\text{re}}^2}{(\dot{A}_{\text{re}}B_{\text{re}} - A_{\text{re}}\dot{B}_{\text{re}})^2}$, $f_{\text{im}} = \frac{NB_{\text{im}}^2 + 2A_{\text{im}}B_{\text{im}}\rho + \sigma_{\text{im}}^2 A_{\text{im}}^2}{(\dot{A}_{\text{im}}B_{\text{im}} - A_{\text{im}}\dot{B}_{\text{im}})^2}$, $\sigma_{\text{re}}^2 = 3N - 4\gamma_1 - 2(-1)^{k_p}(\gamma_{2k_p+1} - \gamma_{2k_p-1})$, $\sigma_{\text{im}}^2 = 3N - 4\gamma_1 + 2(-1)^{k_p}(\gamma_{2k_p+1} - \gamma_{2k_p-1})$, $\rho = (-1)^{k_p}(\gamma_{2k_p+1} + \gamma_{2k_p-1})$ and $\gamma_k = \sin\left(\frac{\pi}{2N}k\right)$. The derivation of asymptotic MSE expression is given in (Appendix D). The analytical complexity of the MSE expression is due to the correlation of noise between neighboring DFT bins due to $2N$-point DFT operation.

4. Numerical results

We compare the performance of the suggested estimator with the state-of-the art estimators. The performance comparisons are conducted at challenging operational conditions of short data records ($N = 16$) and large frequency separation from DFT bins i.e. with an odd valued k_p and a rather small δ due to the definition of $\omega = \frac{2\pi}{2N}(k_p + \delta)$. The signal phase ϕ is independently sampled from uniform distribution in $[0, 2\pi)$ at each Monte Carlo trial. This enables the utilization of HCRB as a performance bound. The Cramer-Rao bound shown in the figures is calculated with the units of $2N$-DFT bins. Since $k_p + \delta = \omega\frac{2N}{2\pi}$, the product of $\sqrt{\text{ACRB}}$ given by (4) and $\frac{2N}{2\pi}$ is the bound for the root mean square error (RMSE) with the unit of $2N$-point DFT-bins.

4.1. Accuracy of iterative inversion

Fig. 3 shows the accuracy of the inverse function mapping method. The unknown frequency is set as $3 + \delta$ bins where δ takes values in $[-0.5, 0.5]$. The Taylor series expansion point of the first iteration is taken as $\delta_0 = 0.25$. From Fig. 3, it is seen that 10 iterations are sufficient to reach the numerical accuracy of the computing platform. In many cases, it suffices to have fewer iterations. For example, if the desired accuracy or the achievable accuracy at a given SNR is on the order of 1/100 of a DFT bin size, one can choose to terminate the scheme at the 6th iteration, given the information in Fig. 3.

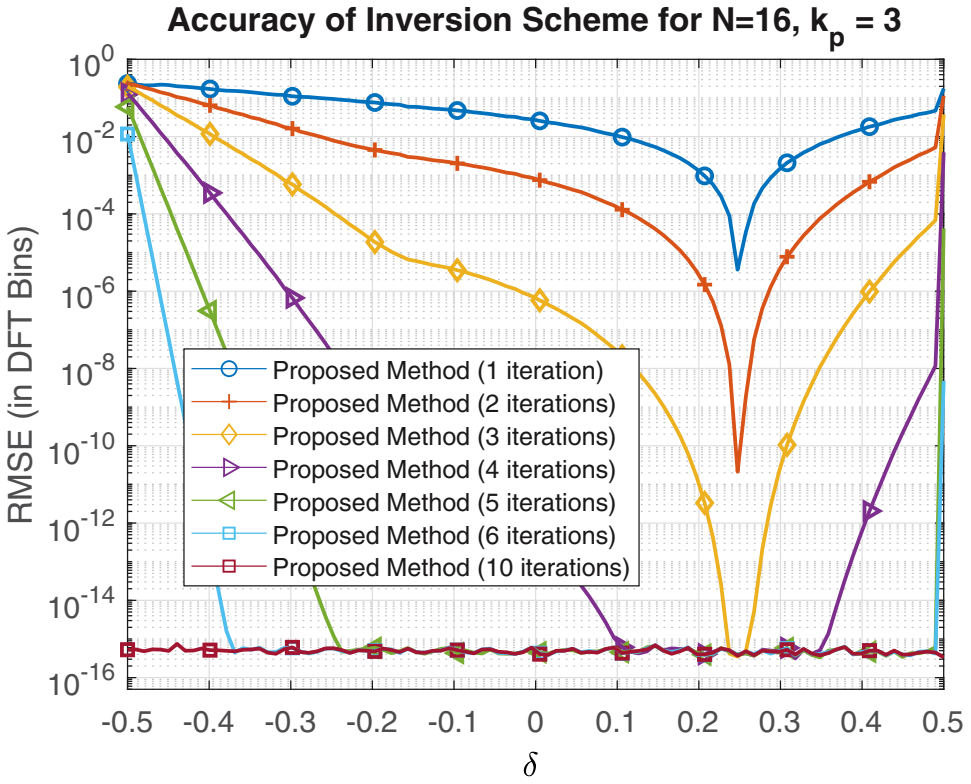

Fig. 3. Accuracy of the iterative inversion scheme for different number of iterations (noise-free operation).

4.2. Estimator RMSE

Fig. 4 shows RMSE of the estimators for a length $N = 16$ input with frequency $k_p + \delta$ DFT bins, where $k_p = 3$ and $\delta = -0.2$. It can seen from Fig. 4 that the method of Djukanovicàims [28] suffers from an error floor due to the estimator bias at high SNR. Suggested method, method of Ye et al. [29] and ML estimator closely track the CRB at a very small SNR gap. We have implemented two versions of the method of Ye et al. [29], denoted as YSA-N and YSA-2N. YSA-N (given in Ye et al. [29]) uses N-point DFT in the coarse localization stage, while YSA-2N (see Algorithm 2 listing) uses $2N$-point DFT[2]. For all practical purposes, estimators except the one of Djukanovicàims act like ML estimator in the high SNR region. The suggested method, YSA-2N and ML estimator perform almost identically at all SNR values.

Algorithm 2: YSA-2N Method, ([29,30] with 2N points).

Input : $r[n]$: N samples of noisy real-valued sinusoid;
Output: $\widehat{\omega} = \frac{2\pi}{N}(\widehat{k} + \widehat{\delta})$ rad./sample;

$R[k]$ =fft$(r[n], 2N)$ ($2N$-point FFT calculation);
$\widehat{m} = \arg\max_{0\le k\le N-1} |R[k]|^2$(locate maxima in spectrum);
$\widehat{k} = \widehat{m}/2$;
Set $\widehat{\delta} = 0$ and $\widehat{a} = 0$;
  for iteration from 1 to Q,
    $X_p = \frac{1}{N}\sum_{n=0}^{N-1} x(n) e^{-j\frac{2\pi}{N}(\widehat{k}+\widehat{\delta}+p)n}$, $p = \pm 0.5$;
    $\widehat{L}_p = \frac{\widehat{a}^*}{N} \frac{1+e^{-j4\pi\widehat{\delta}}}{1-e^{-j\frac{2\pi}{N}(2\widehat{k}+2\widehat{\delta}+p)}}$, and $\widehat{S}_p = X_p - \widehat{L}_p$;
    $\widehat{\delta} = \widehat{\delta} + \frac{1}{2}\mathrm{Re}\left(\frac{\widehat{S}_{0.5}+\widehat{S}_{-0.5}}{\widehat{S}_{0.5}-\widehat{S}_{-0.5}}\right)$;
    $\widehat{a} = \frac{1}{N}\left(\sum_{n=0}^{N-1} x(n) e^{-j\frac{2\pi}{N}(\widehat{k}+\widehat{\delta})n} - \widehat{a}^* \frac{1-e^{j4\pi\widehat{\delta}}}{1-e^{-j\frac{4\pi}{N}(\widehat{k}+\widehat{\delta})}}\right)$;
  end for
Return $\widehat{\omega} = \frac{2\pi}{N}(\widehat{k} + \widehat{\delta})$.

4.3. On fusion operation

Fig. 5 studies the success of the fusion operation by comparing RMSE of $\widehat{\delta}_{\mathrm{re}}$, $\widehat{\delta}_{\mathrm{im}}$ and $\widehat{\delta}_{\mathrm{F}}$. The experiment parameters are $N = 16$, $k_p = 3$, $\delta = -0.2$, SNR $= 30$ dB. Fig. 5 shows RMSE of the estimates as phase ϕ varies in [0,180] degrees. In this experiment, the signal phase is taken as a *non-random parameter* to observe its impact on $\widehat{\delta}_{\mathrm{re}}$ and $\widehat{\delta}_{\mathrm{im}}$.

As noted earlier, depending on the value of $\widetilde{\phi} = \phi + \pi\delta(1 - \frac{1}{N}) - \frac{\pi}{N}k_p$, the input SNR of $\widetilde{R}_{\mathrm{re}}[l]$ and $\widetilde{R}_{\mathrm{im}}[l]$ can vary significantly, affecting the accuracy of the frequency estimates. It is seen that the suggested fusion rule, with the practical fusion coefficient given by (16), successfully combines both estimates so that the final error is almost independent of the signal phase. In Fig. 5, CRB relation for finite N, given in [31, p. 56], is utilized. We note that in this experiment, all unknown parameters are non-random; hence, HCRB is not applicable and ACRB is not accurate for $N = 16$.

4.4. Computational complexity considerations

Numerical results indicate that the performance of suggested invariant function based method, method of Ye et al. [29] (with $2N$-point DFT in the first stage) and the maximum-likelihood method are almost identical for a wide range of SNR values. If

[2] YSA-N is the state-of-art estimator [29,30]. YSA-2N in Algorithm 2 listing is a simple modification of the original method to 2N-DFT points in the first stage which results in an even better performance.

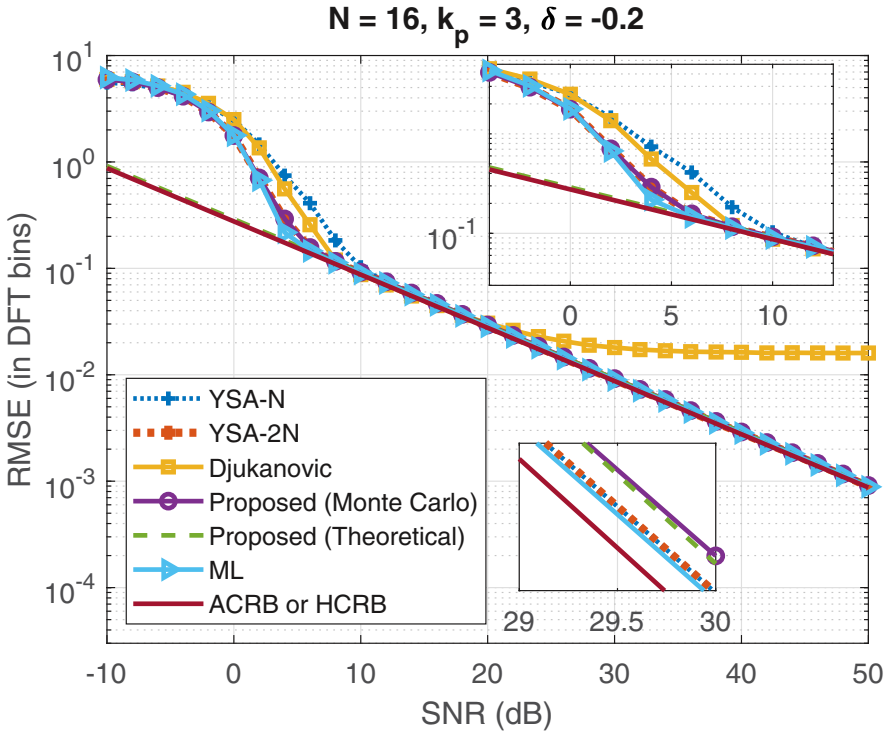

Fig. 4. RMSE comparison of the proposed method with other methods.

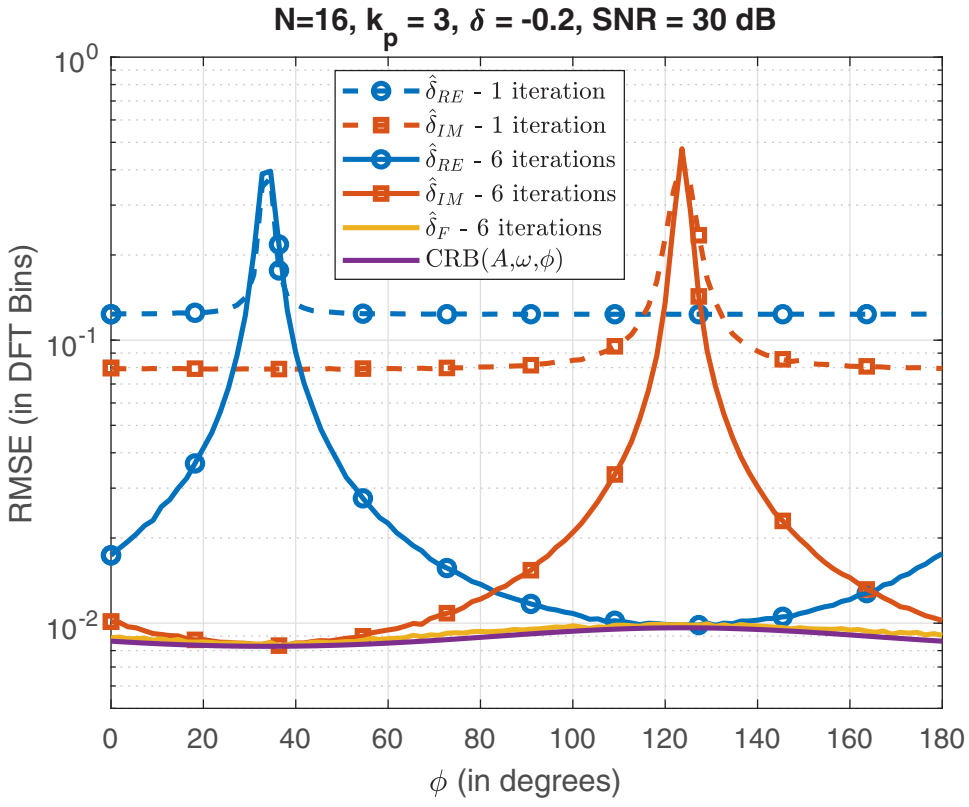

Fig. 5. Estimator accuracy comparison before and after fusion operation.

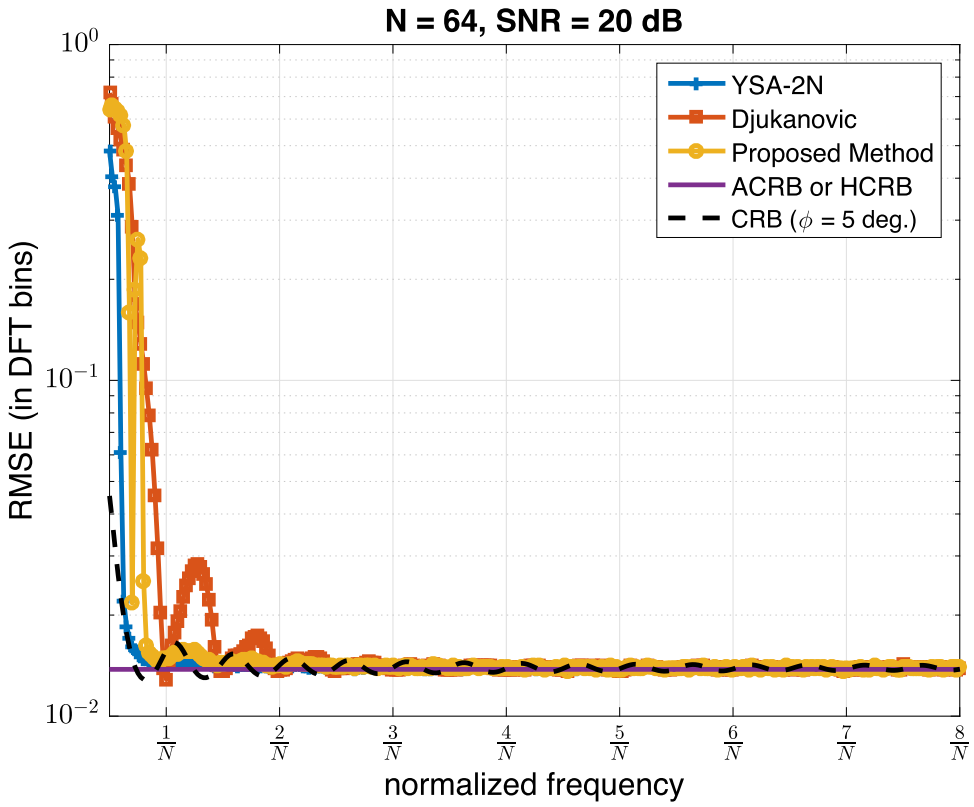

Fig. 6. Comparison of estimators for $N = 64$ and SNR $= 20$ dB at different frequencies.

we compare the computational complexity of these three methods, the maximum likelihood by grid-search requires calculation of very high point DFT's to attain the Cramer-Rao bound especially at high SNR values. The method by Ye et al. (YSA-2N) requires $2N$-point DFT in the first stage and $2N$ complex multiplications per iteration for the calculation of X_p and $\widehat{a}$ given in the lines 6 and 9 of Algorithm 2 listing. Typically, 2 to 5 iterations are required until convergence, [29,30]. The suggested method requires a $2N$-point DFT; evaluation of ratio_{re} and ratio_{im} (line 5 of Algorithm 1 listing) and evaluation of inverse mapping on ratio_{re} and ratio_{im} (lines 6–15 of Algorithm 1 listing). Hence, the computational load of the first stage of both YSA-2N and the proposed method is identical. The proposed method incurs slightly less computation in the second stage due to the absence of a complex amplitude estimation stage present in YSA-2N method. The computational load difference between YSA-2N and the proposed method diminishes for increasing N; since the total computational load will be dominated by the first stage. Note that, in case that $f^{-1}(\cdot)$ mapping can be implemented via a look-up table, the second stage of the proposed method is iteration-free and its computational load is null.

4.5. Cautionary remarks

RMSE results similar to the one given in Fig. 4 can be obtained for different N, k_p and δ values except for extremely low ($k_p \in \{0, 1\}$) and high ($k_p \in \{N-1, N\}$) frequencies. This is essentially due to the special conditions on the DC and the maximum frequency DFT bin. Simply put, the DC bin output is the sum of all input samples which is purely real for the real-valued sinusoid problem. Therefore, the imaginary part of this bin, or ratio_{im}, is of no value for the estimation problem. (It can be observed that the same is also true for the maximum frequency DFT bin.)

Fig. 6 shows the frequency estimation RMSE of different methods for $N = 64$ and SNR $= 20$ dB at various frequencies. As the unknown frequency approaches 0, all methods suffer performance losses due to the model mismatch at the DC bin, as previously discussed. Note that ACRB is not capable of reflecting the performance losses due to its asymptotic definition. In Fig. 6, we have also included the non-asymptotic CRB to illustrate that the performance loss at low frequencies is indeed expected. (In Fig. 6, we present the CRB for the phase angle of $\phi = 5^\circ$; but, the Monte Carlo experiment is conducted with randomly selected phase angles from uniform $[0, 2\pi)$ distribution. The frequency estimation error for the phase angles with a large deviation from ACRB, such as $\phi = 5^\circ$, typically dominate the Monte Carlo results at low frequencies.) Hence, the extreme low and high frequency cases for the real-valued sinusoid frequency estimation problem should be treated individually.

5. Conclusions

We describe an invariant function approach for the parameter estimation problem and apply the approach on the problem of frequency estimation of real-valued sinusoids observed under AWGN noise. The suggested approach results in a very low complexity estimator performing as well as the maximum likelihood estimator in many scenarios. The suggested method can be either implemented via a look-up table resulting in a one-shot estimator or via suggested numerical method without any look-up table storage requirements. We invite readers to conduct additional Monte Carlo runs with the ready-to-use MATLAB implementation of the suggested method in Candan and Celebi [35]. We think that the suggested invariant function approach can be utilized in other parameter estimation problems and can be a computationally efficient alternative to the grid-search based or numerical-search based ML estimators.

Declaration of Competing Interest

The authors declare that they have no known competing financial interests or personal relationships that could have appeared to influence the work reported in this paper.

Appendix A. Maximum likelihood estimator

The maximum likelihood estimator for the frequency ω is given in Kay [31, Eq. (7.65)] and [3]. We present a compact expression in terms of the discrete time Fourier transform (DTFT) of the input.

The maximum likelihood expression can be written as $\arg\max_\omega ||\mathbf{P}_\omega \mathbf{r}||^2$ where $\mathbf{P}_\omega$ is the projection matrix to subspace spanned by $\boldsymbol{c} = [1 \;\; \cos(\omega) \ldots \cos(\omega(N-1))]^T$ and $\boldsymbol{s} = [0 \;\; \sin(\omega) \ldots \sin(\omega(N-1))]^T$, see [31, Eq. (7.65)] for more details. To get an analytical expression for the projection operation, we define $\widehat{\mathbf{s}} = \mathbf{s}_\mathrm{u} + \mathbf{c}_\mathrm{u}$ and $\widehat{\mathbf{c}} = \mathbf{s}_\mathrm{u} - \mathbf{c}_\mathrm{u}$ where $\mathbf{s}_\mathrm{u} = \mathbf{s}/||\mathbf{s}||$, $\mathbf{c}_\mathrm{u} = \mathbf{c}/||\mathbf{c}||$. The vectors $\widehat{\mathbf{s}}$ and $\widehat{\mathbf{c}}$ are orthogonal vectors in the span of $\boldsymbol{s}$ and $\boldsymbol{c}$. By normalizing $\widehat{\mathbf{s}}$ and $\widehat{\mathbf{c}}$ to unit norm; we get an orthonormal set of basis vectors for the span of $\boldsymbol{s}$ and $\boldsymbol{c}$. Hence, the maximum likelihood expression can be written as:

$$\begin{aligned}\widehat{\omega} &= \arg\max_\omega ||\mathbf{P}_\omega \mathbf{r}||^2 \\ &= \arg\max_\omega \frac{(\widehat{\mathbf{s}}^T\mathbf{r})^2}{||\widehat{\mathbf{s}}||^2} + \frac{(\widehat{\mathbf{c}}^T\mathbf{r})^2}{||\widehat{\mathbf{c}}||^2} \qquad \text{(A.1)}\end{aligned}$$

$$= \arg\max_\omega \left[\frac{(\mathbf{s}_\mathrm{u}^T\mathbf{r} + \mathbf{c}_\mathrm{u}^T\mathbf{r})^2}{2(1+\mathbf{s}_\mathrm{u}^T\mathbf{c}_\mathrm{u})} + \frac{(\mathbf{s}_\mathrm{u}^T\mathbf{r} - \mathbf{c}_\mathrm{u}^T\mathbf{r})^2}{2(1-\mathbf{s}_\mathrm{u}^T\mathbf{c}_\mathrm{u})} \right], \qquad \text{(A.2)}$$

where $||\widehat{\mathbf{s}}||^2 = 2(1+\mathbf{s}_\mathrm{u}^T\mathbf{c}_\mathrm{u})$ and $||\widehat{\mathbf{c}}||^2 = 2(1-\mathbf{s}_\mathrm{u}^T\mathbf{c}_\mathrm{u})$. By adding two terms forming the argument of arg max in (A.2) and substituting $\mathbf{s}_\mathrm{u} = \mathbf{s}/||\mathbf{s}||$ and $\mathbf{c}_\mathrm{u} = \mathbf{c}/||\mathbf{c}||$; we get

$$\widehat{\omega} = \arg\max_\omega \frac{(\mathbf{s}^T\mathbf{r})^2||\mathbf{c}||^2 + (\mathbf{c}^T\mathbf{r})^2||\mathbf{s}||^2 - 2(\mathbf{s}^T\mathbf{r})(\mathbf{c}^T\mathbf{r})(\mathbf{s}^T\mathbf{c})}{||\mathbf{s}||^2||\mathbf{c}||^2 - (\mathbf{s}^T\mathbf{c})^2}. \qquad \text{(A.3)}$$

Next, we derive the expressions for $||\mathbf{c}||^2$, $||\mathbf{s}||^2$ and $\mathbf{s}^T\mathbf{c}$ by observing that

$$\begin{aligned}R + jX &= \sum_{n=0}^{N-1} e^{j2\omega n} = \sum_{n=0}^{N-1} \cos(2\omega n) + j\sin(2\omega n) \\ &= e^{j\omega(N-1)} \frac{\sin(\omega N)}{\sin(\omega)} \qquad \text{(A.4)}\end{aligned}$$

and $R = \sum_{n=0}^{N-1}(\cos^2(\omega n) - \sin^2(\omega n)) = ||\mathbf{c}||^2 - ||\mathbf{s}||^2$ and $X = 2\sum_{n=0}^{N-1}\sin(\omega n)\cos(\omega n) = \mathbf{s}^T\mathbf{c}$. Also noting that $||\mathbf{c}||^2 + ||\mathbf{s}||^2 = N$, we get $||\mathbf{c}||^2 = (N+R)/2$, $||\mathbf{s}||^2 = (N-R)/2$ and $\mathbf{s}^T\mathbf{c} = X/2$. By substituting these expressions in (A.3), the ML expression becomes

$$\begin{aligned}\widehat{\omega} &= \arg\max_\omega \frac{2(\mathbf{s}^T\mathbf{r})^2(N+R) + 2(\mathbf{c}^T\mathbf{r})^2(N-R) - 4X(\mathbf{s}^T\mathbf{r})(\mathbf{c}^T\mathbf{r})}{N^2 - R^2 - X^2} \\ &= \arg\max_\omega \frac{2N((\mathbf{s}^T\mathbf{r})^2 + (\mathbf{c}^T\mathbf{r})^2) + 2R((\mathbf{s}^T\mathbf{r})^2 - (\mathbf{c}^T\mathbf{r})^2) - 4X(\mathbf{s}^T\mathbf{r})(\mathbf{c}^T\mathbf{r})}{N^2 - (R^2+X^2)} \\ &= \arg\max_\omega \frac{2N|R(e^{j\omega})|^2 + 2\mathrm{Re}\{R^2(e^{j\omega})(R+jX)\}}{N^2 - (R^2+X^2)} \qquad \text{(A.5)}\end{aligned}$$

where $R(e^{j\omega})$ is the discrete-time Fourier transform (DTFT) of $r[n]$ which is $R(e^{j\omega}) = (\mathbf{s}^T\mathbf{r}) + j(\mathbf{c}^T\mathbf{r})$. Substituting the expression for $R + jX$ and its magnitude square $(R^2 + X^2)$ from (A.4) into the last expression, we finalize the derivation of the ML estimator:

$$\widehat{\omega} = \arg\max_\omega \frac{|R(e^{j\omega})|^2 + \frac{\sin(\omega N)}{N\sin(\omega)}\mathrm{Re}\{R^2(e^{j\omega})e^{j\omega(N-1)}\}}{N - \frac{\sin^2(\omega N)}{N\sin^2(\omega)}}.$$

Appendix B. Independence of $\widehat{\delta}_{re}$ and $\widehat{\delta}_{im}$

The mean values of $\widetilde{R}_{re}[l] = \mathrm{Re}\{\widetilde{R}[l]\}$ and $\widetilde{R}_{im}[l] = \mathrm{Im}\{\widetilde{R}[l]\}$, with $\widetilde{R}[l]$ definition given in (7), have no effect on the statistical properties of these random variables. We take the mean value (the signal component) of the random variables as zero to simplify the derivation and define

$$S_l = \alpha^{k_p+l} \sum_{n=0}^{N-1} e^{-\frac{j2\pi(k_p+l)n}{2N}} w[n] \qquad \text{(B.1)}$$

where $l = k - k_p$, $\alpha = e^{\frac{j\pi(N-1)}{2N}}$. S_l is identical to $\widetilde{R}[l]$, given in (7), in the absence of signal term. To determine the statistical properties of $\widetilde{R}_{re}[l]$ and $\widetilde{R}_{im}[l]$, we first examine the auto-correlation of the random variables:

$$\begin{aligned}E\{S_{l_1}S_{l_2}^*\} &= \alpha^{l_1-l_2} E\left\{ \left(\sum_{n_1=0}^{N-1} e^{-\frac{j2\pi(k_p+l_1)n_1}{2N}} w[n_1] \right) \left(\sum_{n_2=0}^{N-1} e^{\frac{j2\pi(k_p+l_2)n_2}{2N}} w^*[n_2] \right) \right\} \\ &\overset{(a)}{=} \sigma_w^2 \alpha^{l_1-l_2} \sum_{n=0}^{N-1} e^{\frac{j2\pi(l_2-l_1)n}{2N}} \\ &= \sigma_w^2 \alpha^{l_1-l_2} \frac{1 - e^{\frac{j2\pi(l_2-l_1)}{2}}}{1 - e^{\frac{j2\pi(l_2-l_1)}{2N}}} \\ &= \sigma_w^2 \alpha^{l_1-l_2} e^{-j\frac{\pi}{2N}(l_2-l_1)(N-1)} \frac{\sin\left(\frac{\pi}{2}(l_2-l_1)\right)}{\sin\left(\frac{\pi}{2N}(l_2-l_1)\right)} \\ &= \sigma_w^2 \frac{\sin\left(\frac{\pi}{2}(l_2-l_1)\right)}{\sin\left(\frac{\pi}{2N}(l_2-l_1)\right)} \triangleq \sigma_w^2 d(l_2-l_1) \qquad \text{(B.2)}\end{aligned}$$

where the function $d(x) = \sin\left(\frac{\pi}{2}x\right)/\sin\left(\frac{\pi}{2N}x\right)$ is introduced in the last line of (B.2).

By following the steps of (B.2) almost verbatim, it is also possible to show that $E\{S_{l_1}S_{l_2}\} = \sigma_w^2 d(2k_p + l_1 + l_2)$. A rather surprising results is that after the phase multiplication in the step 3 of Algorithm 1 listing, both $E\{S_{l_1}S_{l_2}^*\}$ and $E\{S_{l_1}S_{l_2}\}$ becomes a real-valued function.

The covariance of $\widetilde{R}_{re}[l_1]$ and $\widetilde{R}_{re}[l_2]$ can be written as

$$\begin{aligned}E\{\widetilde{R}_{re}[l_1]\widetilde{R}_{re}[l_2]\} &= E\{\mathrm{Re}\{S_{l_1}\}\mathrm{Re}\{S_{l_2}\}\} \qquad \text{(B.3)} \\ &= \frac{1}{4}E\{(S_{l_1} + S_{l_1}^*)(S_{l_2} + S_{l_2}^*)\} \\ &= \frac{1}{2}\mathrm{Re}\{E\{(S_{l_1} + S_{l_1}^*)S_{l_2}\}\} \\ &= \frac{\sigma_w^2}{2}[d(2k_p + l_1 + l_2) + d(l_1 - l_2)].\end{aligned}$$

Note that when $l_1 - l_2$ is a non-zero even number, $E\{\widetilde{R}_{re}[l_1]\widetilde{R}_{re}[l_2]\}$ reduces to zero as expected. Following similar lines of derivations, we can also get $E\{\widetilde{R}_{im}[l_1]\widetilde{R}_{im}[l_2]\} = \frac{\sigma_w^2}{2}[-d(2k_p + l_1 + l_2) + d(l_1 - l_2)]$.

The covariance of $\widetilde{R}_{re}[l_1]$ and $\widetilde{R}_{im}[l_2]$ can also be established as

$$\begin{aligned}E\{\widetilde{R}_{re}[l_1]\widetilde{R}_{im}[l_2]\} &= \frac{1}{4j}E\{(S_{l_1} + S_{l_1}^*)(S_{l_2} - S_{l_2}^*)\} \\ &= \frac{1}{2}\mathrm{Im}\{E\{(S_{l_1} + S_{l_1}^*)S_{l_2}\}\} = 0. \qquad \text{(B.4)}\end{aligned}$$

Hence, the real and imaginary parts of $\widetilde{R}[l]$ are uncorrelated for all l. Since these variables are jointly Gaussian distributed, the uncorrelatedness implies independence. Once the independence of $\widetilde{R}_{re}[l]$ and $\widetilde{R}_{im}[l]$ are established, the fine frequency estimates ($\widehat{\delta}_{re}$ and $\widehat{\delta}_{im}$), which are derived from real and imaginary parts of $\widetilde{R}[l]$, are also independent random variables.

Appendix C. On fusion coefficient calculation

The suggested fusion coefficient is given as $\alpha \triangleq \frac{\widetilde{R}^2_{\rm re}[0]}{\widetilde{R}^2_{\rm re}[0]+\widetilde{R}^2_{\rm im}[0]} = \left(1+\left(\frac{\widetilde{R}_{\rm im}[0]}{\widetilde{R}_{\rm re}[0]}\right)^2\right)^{-1}$. Here we provide the details on the ratio $\widetilde{R}_{\rm im}[0]/\widetilde{R}_{\rm re}[0]$ generating the fusion coefficient. Below, it is shown that

$$\frac{\widetilde{R}_{\rm im}[0]}{\widetilde{R}_{\rm re}[0]} = \tan(\widetilde{\phi}) \underbrace{\left[\tan\left(\frac{\pi k_p}{2N}\right)\cot\left(\frac{\pi(k_p+\delta)}{2N}\right)\right]^p}_{\approx 1} \approx \tan(\widetilde{\phi}), \tag{C.1}$$

where $p=(-1)^{\widehat{k}_p}$ is the parity of $\widehat{k}_p$, taking the value of 1 or -1 depending on $\widehat{k}_p$ being an even or odd integer.

By substituting the definitions for $\widetilde{R}_{\rm re}[0]$ and $\widetilde{R}_{\rm im}[0]$ from (8) into $\frac{\widetilde{R}_{\rm im}[0]}{\widetilde{R}_{\rm re}[0]}$, we get

$$\frac{\widetilde{R}_{\rm im}[0]}{\widetilde{R}_{\rm re}[0]} = \tan(\widetilde{\phi})\frac{\sin(\frac{B}{N})\sin(A)-\sin(\frac{A}{N})\sin(B)}{\sin(\frac{B}{N})\sin(A)+\sin(\frac{A}{N})\sin(B)} \tag{C.2}$$

with $A=\frac{\pi}{2}\delta$ and $B=\frac{\pi}{2}(2k_p+\delta)$. We note that $\sin(B)=\sin(\pi k_p+\frac{\pi}{2}\delta)=(-1)^{k_p}\sin(A)$. Upon the substitution of $\sin(B)=(-1)^{k_p}\sin(A)$, into (C.2), we get:

$$\frac{\widetilde{R}_{\rm im}[0]}{\widetilde{R}_{\rm re}[0]}\cot(\widetilde{\phi}) = \frac{\sin(\frac{B}{N})-(-1)^{k_p}\sin(\frac{A}{N})}{\sin(\frac{B}{N})+(-1)^{k_p}\sin(\frac{A}{N})}. \tag{C.3}$$

Assuming, for now, k_p is an even number, (C.3) reduces to

$$\begin{aligned}\frac{\widetilde{R}_{\rm im}[0]}{\widetilde{R}_{\rm re}[0]}\cot(\widetilde{\phi}) &= \frac{\sin(\frac{B}{N})-\sin(\frac{A}{N})}{\sin(\frac{B}{N})+\sin(\frac{A}{N})} = \frac{\sin(\frac{B-A}{2N})\cos(\frac{B+A}{2N})}{\sin(\frac{B+A}{2N})\cos(\frac{B-A}{2N})}\\ &= \tan\left(\frac{B-A}{2N}\right)\cot\left(\frac{B+A}{2N}\right).\end{aligned} \tag{C.4}$$

Inserting $\frac{B-A}{2N}=\frac{\pi k_p}{2N}$ and $\frac{B+A}{2N}=\frac{\pi(k_p+\delta)}{2N}$ into (C.4), results in

$$\frac{\widetilde{R}_{\rm im}[0]}{\widetilde{R}_{\rm re}[0]} = \tan(\widetilde{\phi})\tan\left(\frac{\pi k_p}{2N}\right)\cot\left(\frac{\pi(k_p+\delta)}{2N}\right). \tag{C.5}$$

When k_p is an odd number, the numerator of the ratio on the right side of (C.3) is swapped with its the denominator and we have $\frac{\widetilde{R}_{\rm im}[0]}{\widetilde{R}_{\rm re}[0]} = \tan(\widetilde{\phi})\left[\tan\left(\frac{\pi k_p}{2N}\right)\cot\left(\frac{\pi(k_p+\delta)}{2N}\right)\right]^{-1}$. Both cases can be summarized as in (C.1).

Appendix D. Derivation of asymptotic MSE expression

To derive the asymptotic MSE expression, we assume that noise variance σ_w^2 is sufficiently low such that ratio$_{\rm re}$ given in (9) can be approximated as ratio$_{\rm re} \approx f_{\rm re}(\delta)+$(equivalent-noise). Here the term (equivalent-noise) denotes the equivalent additive noise formed by ignoring noise-cross-noise terms, with the low noise variance (high SNR) assumption.

In the absence of noise, we have ratio$_{\rm re}$ is $f_{\rm re}(\delta) \triangleq$ ratio$_{\rm re} = \frac{\widetilde{R}_{\rm re}[1]-\widetilde{R}_{\rm re}[-1]}{2\widetilde{R}_{\rm re}[0]-\widetilde{R}_{\rm re}[1]-\widetilde{R}_{\rm re}[-1]} = A_{\rm re}/B_{\rm re}$ where we have assumed $\delta-\delta_0\approx 0$ in (12), i.e. the iterative inversion scheme is executed until convergence. In the presence of noise, ratio$_{\rm re}$ becomes

$$\text{ratio}_{\rm re} = \frac{\frac{A\cos(\widetilde{\phi})}{2}A_{\rm re}+w^{\rm re}_{\rm num}}{\frac{A\cos(\widetilde{\phi})}{2}B_{\rm re}+w^{\rm re}_{\rm denum}}, \tag{D.1}$$

where $w^{\rm re}_{\rm num}=\text{Re}\{S_1\}-\text{Re}\{S_{-1}\}$ and $w^{\rm re}_{\rm denum}=2\text{Re}\{S_0\}-\text{Re}\{S_1\}-\text{Re}\{S_{-1}\}$. Here, we use the random variable S_l defined in (Appendix B). It is clear that $w^{\rm re}_{\rm num}$ and $w^{\rm re}_{\rm denum}$ are jointly Gaussian distributed zero-mean random variables. Using the results of (Appendix B), we can express the marginal distributions as $w^{\rm re}_{\rm num} \sim \mathcal{N}(0,\, N\sigma_w^2)$ and

$$w^{\rm re}_{\rm denum} \sim \mathcal{N}\left(0,\, \sigma_w^2\left[3N-\frac{4}{\sin(\frac{\pi}{2N})}-2(-1)^{k_p}\left(\frac{1}{\sin(\frac{\pi(2k_p+1)}{2N})}-\frac{1}{\sin(\frac{\pi(2k_p-1)}{2N})}\right)\right]\right).$$

and the cross-correlation of $w^{\rm re}_{\rm num}$ and $w^{\rm re}_{\rm denum}$ as

$$E\{w^{\rm re}_{\rm num}w^{\rm re}_{\rm denum}\} = \sigma_w^2(-1)^{k_p}\left(\frac{1}{\sin(\frac{\pi(2k_p+1)}{2N})}+\frac{1}{\sin(\frac{\pi(2k_p-1)}{2N})}\right).$$

To get the equivalent noise term, we express ratio$_{\rm re}$ as

$$\begin{aligned}\text{ratio}_{\rm re} &= \frac{\frac{A_{\rm re}}{B_{\rm re}}+\frac{w^{\rm re}_{\rm num}}{\frac{A\cos(\widetilde{\phi})}{2}B_{\rm re}}}{1+\frac{w^{\rm re}_{\rm denum}}{\frac{A\cos(\widetilde{\phi})}{2}B_{\rm re}}} = \frac{\frac{A_{\rm re}}{B_{\rm re}}+\widetilde{w}^{\rm re}_{\rm num}}{1+\widetilde{w}^{\rm re}_{\rm denum}}\frac{1-\widetilde{w}^{\rm re}_{\rm denum}}{1-\widetilde{w}^{\rm re}_{\rm denum}}\\ &\approx \frac{A_{\rm re}}{B_{\rm re}}+\widetilde{w}^{\rm re}_{\rm num}-\frac{A_{\rm re}}{B_{\rm re}}\widetilde{w}^{\rm re}_{\rm denum},\end{aligned}$$

where $\widetilde{w}^{\rm re}_{\rm num}=2w^{\rm re}_{\rm num}/(A\cos(\widetilde{\phi})B_{\rm re})$ and $\widetilde{w}^{\rm re}_{\rm denum}=2w^{\rm re}_{\rm denum}/(A\cos(\widetilde{\phi})B_{\rm re})$ and $w^{\rm re}_{\rm num}-\frac{A_{\rm re}}{B_{\rm re}}$ is the equivalent noise term which is formed by ignoring second powers of noise at the numerator and denominator of the ratio in (D.2).

The arguments given above when repeated almost verbatim for the ratio$_{\rm im}$ constructed from the imaginary part of $\widetilde{R}[l]$ (step 4 of Algorithm 1), we get the ratio$_{\rm im} \approx \frac{A_{\rm im}}{B_{\rm im}}+\widetilde{w}^{\rm im}_{\rm num}-\frac{A_{\rm im}}{B_{\rm im}}\widetilde{w}^{\rm im}_{\rm denum}$ where $A_{\rm im}, B_{\rm im}$ and $\widetilde{w}^{\rm im}_{\rm num}, \widetilde{w}^{\rm im}_{\rm denum}$ are similarly defined.

Following (14), the asymtotic mean squared error expressions for $\widehat{\delta}_{\rm re}$ and $\widehat{\delta}_{\rm im}$ can be written as $c^2_{N_{\rm re}}(\text{var}(\widetilde{w}^{\rm re}_{\rm num})+\frac{A^2_{\rm re}}{B^2_{\rm re}}\text{var}(\widetilde{w}^{\rm re}_{\rm denum})-2\frac{A_{\rm re}}{B_{\rm re}}E\{\widetilde{w}^{\rm re}_{\rm num}\widetilde{w}^{\rm re}_{\rm denum}\})$ and $c^2_{N_{\rm im}}(\text{var}(\widetilde{w}^{\rm im}_{\rm num})+\frac{A^2_{\rm im}}{B^2_{\rm im}}\text{var}(\widetilde{w}^{\rm im}_{\rm denum})-2\frac{A_{\rm im}}{B_{\rm im}}E\{\widetilde{w}^{\rm im}_{\rm num}\widetilde{w}^{\rm im}_{\rm denum}\})$ respectively where $c_{N_{\rm re}}=\frac{B^2_{\rm re}}{A_{\rm re}B_{\rm re}-A_{\rm re}B_{\rm re}}$ and $c_{N_{\rm im}}=\frac{B^2_{\rm im}}{A_{\rm im}B_{\rm im}-A_{\rm im}B_{\rm im}}$.

With the fusion rule of $\widehat{\delta}_F=\cos^2(\widetilde{\phi})\widehat{\delta}_{\rm re}+\sin^2(\widetilde{\phi})\widehat{\delta}_{\rm im}$ (see Appendix C), the asymptotic MSE becomes

$$\begin{aligned}E[(\delta-\widehat{\delta}_F)^2] &= \frac{2[E\{\cos^2(\widetilde{\phi})\}f_1+E\{\sin^2(\widetilde{\phi})\}f_2]}{\text{SNR}}\\ &= \frac{f_{re}+f_{im}}{\text{SNR}}\end{aligned}$$

where $f_{\rm re}=\frac{NB^2_{\rm re}-2A_{\rm re}B_{\rm re}\rho+\sigma^2_{\rm re}A^2_{\rm re}}{(A_{\rm re}B_{\rm re}-A_{\rm re}B_{\rm re})^2}$, $f_{\rm im}=\frac{NB^2_{\rm im}+2A_{\rm im}B_{\rm im}\rho+\sigma^2_{\rm im}A^2_{\rm im}}{(A_{\rm im}B_{\rm im}-A_{\rm im}B_{\rm im})^2}$, $\gamma_k=\sin\left(\frac{\pi}{2N}k\right)$, $\sigma^2_{\rm re}=3N-4\gamma_1-2(-1)^{k_p}(\gamma_{2k_p+1}-\gamma_{2k_p-1})$, $\sigma^2_{\rm im}=3N-4\gamma_1+2(-1)^{k_p}(\gamma_{2k_p+1}-\gamma_{2k_p-1})$, $\rho=(-1)^{k_p}(\gamma_{2k_p+1}+\gamma_{2k_p-1})$.

An inspection of $f_{\rm re}$ and $f_{\rm im}$ reveals that the numerator and denominator of both ratios increase with N^3 and N^4 as $N\to\infty$, respectively. Hence, as $N\to\infty$, that is the asymptotic MSE $=\frac{f_{re}+f_{im}}{\text{SNR}}$ tends to $\gamma/(\text{SNR}\times N)$ (with the units of DFT-bin^2) where the factor γ is a scenario specific parameter, with a dependency on δ that determines the constant gap of the estimator from the ACRB in the high SNR region.

CRediT authorship contribution statement

Çağatay Candan: Conceptualization, Formal analysis, Software, Writing - review & editing, Supervision. **Utku Çelebi:** Software, Formal analysis, Writing - original draft, Visualization.

References

[1] P. Stoica, R. Moses, Spectral Analysis of Signals, Prentice Hall, 2005.

[2] P. Stoica, List of references on spectral line analysis, Signal Process. 31 (3) (1993) 329–340, doi:10.1016/0165-1684(93)90090-W.
[3] R. Kenefic, A. Nuttall, Maximum likelihood estimation of the parameters of a tone using real discrete data, IEEE J. Ocean. Eng. 12 (1) (1987) 279–280, doi:10.1109/JOE.1987.1145230.
[4] H.C. So, K.W. Chan, Y.T. Chan, K.C. Ho, Linear prediction approach for efficient frequency estimation of multiple real sinusoids: algorithms and analyses, IEEE Trans. Signal Process. 53 (7) (2005) 2290–2305, doi:10.1109/TSP.2005.849154.
[5] H.C. So, F.K.W. Chan, W. Sun, Efficient frequency estimation of a single real tone based on principal singular value decomposition, Digit. Signal Process. 22 (6) (2012) 1005–1009, doi:10.1016/j.dsp.2012.05.010.
[6] B.G. Quinn, Estimating frequency by interpolation using Fourier coefficients, IEEE Trans. Signal Process. 42 (5) (1994) 1264–1268, doi:10.1109/78.295186.
[7] B.G. Quinn, E.J. Hannan, The Estimation and Tracking of Frequency, Cambridge University Press, 2001.
[8] M.D. Macleod, Fast nearly ML estimation of the parameters of real or complex single tones or resolved multiple tones, IEEE Trans. Signal Process. 46 (1) (1998) 141–148, doi:10.1109/78.651200.
[9] E. Aboutanios, B. Mulgrew, Iterative frequency estimation by interpolation on Fourier coefficients, IEEE Trans. Signal Process. 53 (4) (2005) 1237–1242, doi:10.1109/TSP.2005.843719.
[10] E. Jacobsen, P. Kootsookos, Fast, accurate frequency estimators, IEEE Signal Process. Mag. 24 (3) (2007) 123–125, doi:10.1109/MSP.2007.361611.
[11] C. Candan, A method for fine resolution frequency estimation from three DFT samples, IEEE Signal Process. Lett. 18 (6) (2011) 351–354, doi:10.1109/LSP.2011.2136378.
[12] C. Candan, Analysis and further improvement of fine resolution frequency estimation method from three DFT samples, IEEE Signal Process. Lett. 20 (9) (2013) 913–916, doi:10.1109/LSP.2013.2273616.
[13] J.-R. Liao, S. Lo, Analytical solutions for frequency estimators by interpolation of DFT coefficients, Signal Process. 100 (2014) 93–100, doi:10.1016/j.sigpro.2014.01.012.
[14] U. Orguner, C. Candan, A fine-resolution frequency estimator using an arbitrary number of DFT coefficients, Signal Process. 105 (2014) 17–21, doi:10.1016/j.sigpro.2014.05.013.
[15] D. Belega, D. Petri, Frequency estimation by two- or three-point interpolated Fourier algorithms based on cosine windows, Signal Process. 117 (2015) 115–125, doi:10.1016/j.sigpro.2015.05.005.
[16] L. Fan, G. Qi, Frequency estimator of sinusoid based on interpolation of three DFT spectral lines, Signal Process. 144 (2018) 52–60, doi:10.1016/j.sigpro.2017.09.028.
[17] Y. Chen, A.H.C. Ko, W.S. Tam, C.W. Kok, H.C. So, Non-iterative DOA estimation using discrete Fourier transform interpolation, IEEE Access 7 (2019) 55620–55630, doi:10.1109/ACCESS.2019.2913747.
[18] P.M. Woodward, Probability and Information Theory, With Applications to Radar, McGraw-Hill, New York, 1955.
[19] V.A. Kotelnikov, The Theory of Optimum Noise Immunity, McGraw-Hill, New York, 1959.
[20] H.L.V. Trees, Detection, Estimation and Modulation Theory, part 1, John Wiley - Sons, 1971.
[21] M.S. Bartlett, Inference and stochastic processes, J. R. Stat. Soc. Ser. A 130 (4) (1967) 457–478.
[22] D.C. Rife, G.A. Vincent, Use of the discrete Fourier transform in the measurement of frequencies and levels of tones, Bell Syst. Tech. J. 49 (2) (1970) 197–228, doi:10.1002/j.1538-7305.1970.tb01766.x.
[23] D. Rife, R. Boorstyn, Single tone parameter estimation from discrete-time observations, IEEE Trans. Inf. Theory 20 (5) (1974) 591–598, doi:10.1109/TIT.1974.1055282.
[24] B.G. Quinn, Estimation of frequency, amplitude, and phase from the DFT of a time series, IEEE Trans. Signal Process. 45 (3) (1997) 814–817, doi:10.1109/78.558515.
[25] E. Aboutanios, Frequency Estimation for Low Earth Orbit Satellites, Univ. of Technology, Sydney, Australia, 2002 Ph.D. thesis.
[26] Y.T. Chan, J.M.M. Lavoie, J.B. Plant, A parameter estimation approach to estimation of frequencies of sinusoids, IEEE Trans. Acoust. Speech Signal Process. 29 (2) (1981) 214–219, doi:10.1109/TASSP.1981.1163543.
[27] H.C. So, Y.T. Chan, K.C. Ho, Y. Chen, Simple formulas for bias and mean square error computation, IEEE Signal Process. Mag. 30 (4) (2013) 162–165, doi:10.1109/MSP.2013.2254600.
[28] S. Djukanovicàims, An accurate method for frequency estimation of a real sinusoid, IEEE Signal Process. Lett. 23 (7) (2016) 915–918, doi:10.1109/LSP.2016.2564102.
[29] S. Ye, J. Sun, E. Aboutanios, On the estimation of the parameters of a real sinusoid in noise, IEEE Signal Process. Lett. 24 (5) (2017) 638–642, doi:10.1109/LSP.2017.2684223.
[30] S. Ye, J. Sun, E. Aboutanios, Corrections to “On the estimation of the parameters of a real sinusoid in noise”, IEEE Signal Process. Lett. 25 (7) (2018), doi:10.1109/LSP.2018.2846138. 1115–1115
[31] S.M. Kay, Fundamentals of Statistical Signal Processing, Volume 1: Estimation Theory, Prentice Hall, 1993.
[32] F. Gini, R. Reggiannini, On the use of Cramer-Rao-like bounds in the presence of random nuisance parameters, IEEE Trans. Commun. 48 (12) (2000) 2120–2126, doi:10.1109/26.891222.
[33] B.G. Quinn, P.J. Kootsookos, Threshold behavior of the maximum likelihood estimator of frequency, IEEE Trans. Signal Process. 42 (11) (1994) 3291–3294, doi:10.1109/78.330402.
[34] F. Athley, Threshold region performance of maximum likelihood direction of arrival estimators, IEEE Trans. Signal Process. 53 (4) (2005) 1359–1373, doi:10.1109/TSP.2005.843717.
[35] C. Candan, U. Celebi, Fine Frequency Estimation For Real-Valued Sinusoidal Signals (Matlab, Code) (2020), doi:10.24433/CO.a8c232cd-7d0d-4eff-8347-de80630f2a52.
[36] B.G. Quinn, Recent advances in rapid frequency estimation, Digit. Signal Process. 19 (6) (2009) 942–948, doi:10.1016/j.dsp.2008.04.004. (DASP'06 - Defense Applications of Signal Processing)